

Parallelizing Maximal Clique Enumeration on GPUs

Mohammad Almasri*
 almasri3@illinois.edu
 University of Illinois at
 Urbana-Champaign
 USA

Rakesh Nagi
 nagi@illinois.edu
 University of Illinois at
 Urbana-Champaign
 USA

Yen-Hsiang Chang*
 yhchang3@illinois.edu
 University of Illinois at
 Urbana-Champaign
 USA

Jinjun Xiong
 jinjun@buffalo.edu
 University at Buffalo
 USA

Izzat El Hajj
 izzat.elhajj@aub.edu.lb
 American University of Beirut
 Lebanon

Wen-mei Hwu
 w-hwu@illinois.edu
 University of Illinois at
 Urbana-Champaign, NVIDIA
 USA

Abstract

We present a GPU solution for exact maximal clique enumeration (MCE) that performs a search tree traversal following the Bron-Kerbosch algorithm. Prior works on parallelizing MCE on GPUs perform a breadth-first traversal of the tree, which has limited scalability because of the explosion in the number of tree nodes at deep levels. We propose to parallelize MCE on GPUs by performing depth-first traversal of independent subtrees in parallel. Since MCE suffers from high load imbalance and memory capacity requirements, we propose a worker list for dynamic load balancing, as well as partial induced subgraphs and a compact representation of excluded vertex sets to regulate memory consumption. Our evaluation shows that our GPU implementation on a single GPU outperforms the state-of-the-art parallel CPU implementation by a geometric mean of $4.9\times$ (up to $16.7\times$), and scales efficiently to multiple GPUs. Our code will be open-sourced to enable further research on accelerating MCE.

1 Introduction

A clique in a graph is a complete subgraph where every vertex in the subgraph is connected to every other vertex with an edge. A maximal clique is a clique that cannot be further expanded by including one more vertex. MCE aims to find all the maximal cliques in a graph, which has a wide variety of applications in numerous domains such as community detection [19, 25, 30, 44], recommender systems [46, 63], graph compression and partitioning [27, 38, 54, 55], prediction of protein functions in protein interaction networks [15, 51, 70, 71], finding gene similarities in gene co-expression networks [21, 59], and identifying price fluctuations in finance networks [8].

One of the most widely used algorithms for solving MCE exactly is the Bron-Kerbosch algorithm [9]. The algorithm involves traversing a search tree that branches from parent nodes representing smaller cliques to child nodes representing larger cliques that contain them until maximal cliques

are found. Prior works on parallelizing MCE on GPUs perform a breadth-first traversal of the search tree [5, 35, 40, 69]. However, this approach does not scale well for large graphs because of the explosion in the number of search tree nodes that need to be tracked as the tree level gets deeper. To overcome this limitation, we propose to parallelize MCE on GPUs by assigning independent subtrees to different thread blocks and having the threads within each block collaboratively perform a depth-first traversal of the block's subtree.

The approach of performing per-block depth-first traversal of independent subtrees has been applied by prior works to related problems such as k -clique counting [3] and subgraph matching [11]. However, MCE presents two key scalability challenges that are less of a concern in related problems. The first challenge is that the MCE search tree is substantially more imbalanced, which means that assigning independent subtrees to different thread blocks suffers from high load imbalance. The second challenge is that MCE requires substantially more memory capacity to track the vertices excluded at each level of the traversal to test for the maximality of a clique. These two challenges are particularly critical on GPUs in contrast with CPUs. GPUs are more sensitive to load imbalance due to their massively parallel nature. Moreover, GPUs typically have a smaller memory capacity than CPUs while putting more pressure on the memory capacity by traversing a larger number of subtrees in parallel.

In this paper, we propose a novel solution for accelerating MCE on GPUs that employs various techniques to address the load imbalance and memory capacity challenges that MCE imposes. We propose a worker list to enable thread blocks with large subtrees to offload branches of their subtrees to other thread blocks with low overhead. We propose using partial induced subgraphs to avoid the latency and memory capacity overhead of constructing full induced subgraphs with information about excluded vertices. We propose a compact representation of the sets of excluded vertices that distinguishes between the part of each set that needs to be stored separately for each level, and the part that monotonically shrinks and can be reused across levels. We also

*Both authors contributed equally to this research.

apply several optimizations used in prior works on related problems such as binary encoding of the induced subgraph and partitioning work at subwarp granularity [3].

Our evaluation shows that our parallel GPU implementation executing on a single server-grade GPU outperforms the state-of-the-art parallel CPU implementation [7] executing on a server-grade CPU by a geometric mean of $4.9\times$ (up to $16.7\times$). We also show that our worker list approach is effective at achieving load balance with low overhead, and enables efficient scaling to multiple GPUs. Our code will be open-sourced for reproducibility and to enable further research on accelerating MCE.

2 Background

2.1 Maximal Clique Enumeration

Let $G = (V, E)$ be a simple undirected graph where V is the set of vertices in G and E is the set of edges in G . The *neighborhood* of a vertex $v \in V$ is the set of vertices adjacent to v , denoted by $N(v)$. A *clique* in G is a complete subgraph of G where every vertex is connected to every other vertex with an edge. A *maximal clique* in G is a clique that cannot be further expanded by including one more vertex. In other words, a maximal clique is a clique that is not contained in a larger clique. For example, the graph in Figure 1(a) has two maximal cliques: ABCD and AEF. On the other hand, ABC, ABD, ACD, and BCD are not maximal cliques because they are all contained inside of ABCD.

MCE aims to find all the maximal cliques in a graph. We tackle MCE as an exact matching problem, which means that we enumerate all maximal cliques in the graph and do not apply any approximations or graph sampling. One of the most widely used algorithms for exact MCE is the Bron-Kerbosch algorithm [9]. In the rest of this section, we describe three variants of this algorithm: Bron-Kerbosch (Section 2.2), Bron-Kerbosch with pivoting (Section 2.3), and Bron-Kerbosch with independent first-level subtrees, degeneracy ordering, and induced subgraphs (Section 2.4).

2.2 Bron-Kerbosch

The Bron-Kerbosch algorithm [9] is a backtracking algorithm that traverses a search tree to find maximal cliques. The search tree branches from parent nodes representing smaller cliques to child nodes representing larger cliques that contain them until maximal cliques are found. While searching, the algorithm maintains three disjoint sets for each tree node: result (R), possible (P), and exclude (X). R is the set of vertices in the clique currently being explored. P and X together contain the common neighbors of the vertices in R . P is the set of common neighbors that can still be added to the clique in R in the current branch of the tree. X is the set of common neighbors that are excluded from the maximal clique being searched for in the current branch of the tree because they have already been considered in another branch of the tree.

Algorithm 1 shows the pseudocode for the Bron-Kerbosch algorithm, and Figure 1(c) shows how this algorithm is applied to the example graph in Figure 1(a). In the initial call to BRONKERBOSCH, R is empty, P contains all the vertices in the graph, and X is empty. The recursive step (lines 4-7) iterates over all the vertices v in the set P . At the recursive call (line 5), v is added to the solution R , and P and X are intersected with $N(v)$ to remove non-neighbors of v . After returning from the call, all maximal cliques containing the vertices in $R \cup \{v\}$ have been found. To avoid finding the same cliques again, v is excluded from the search in later subtrees at the same level by removing v from P (line 6) and adding to X (line 7) before proceeding to the next loop iteration.

Algorithm 1 Bron-Kerbosch algorithm

```

1: procedure BRONKERBOSCH( $G, R, P, X$ )
2:   if  $P$  and  $X$  are both empty then
3:      $R$  is a maximal clique
4:   for  $v \in P$  do
5:     BRONKERBOSCH( $G, R \cup \{v\}, P \cap N(v), X \cap N(v)$ )
6:      $P = P - \{v\}$ 
7:      $X = X \cup \{v\}$ 

```

The recursion stops when P is empty, which means that there are no more vertices that can be added to the clique in R . If P and X are both empty (line 2), then the vertices in R have no common neighbors, which means that R represents a maximal clique (line 3). If P is empty but X is not empty, then the vertices in R do have common neighbors (those in X) and R is not a maximal clique. However, the search stops because the common neighbors in X are excluded from the search on this tree branch, which means that any maximal clique containing R has already been found in other branches.

2.3 Bron-Kerbosch with Pivoting

It is clear from Figure 1(c) that there can be many branches in the search tree that are not successful at finding a maximal clique because the clique is found by other branches. To avoid some of the unsuccessful branches, Bron and Kerbosch introduce *pivoting* [9]. Algorithm 2 shows the pseudocode for the Bron-Kerbosch algorithm with pivoting, and Figure 1(d) shows how this algorithm is applied to the example graph in Figure 1(a). The difference from Algorithm 1 is that in Algorithm 2, a *pivot vertex* is selected prior to branching (line 4) and the neighbors of the pivot vertex are excluded from the branching (line 5). Notice how the search tree in Figure 1(d) with pivoting has substantially fewer branches than the tree in Figure 1(c) without pivoting.

The intuition behind pivoting is that any maximal clique that includes the pivot vertex and its neighbor will be found by the branch that adds the pivot vertex to R . On the other hand, any maximal clique that does not include the pivot vertex but includes its neighbor must include a non-neighbor of the pivot vertex, and will be found by the branches that

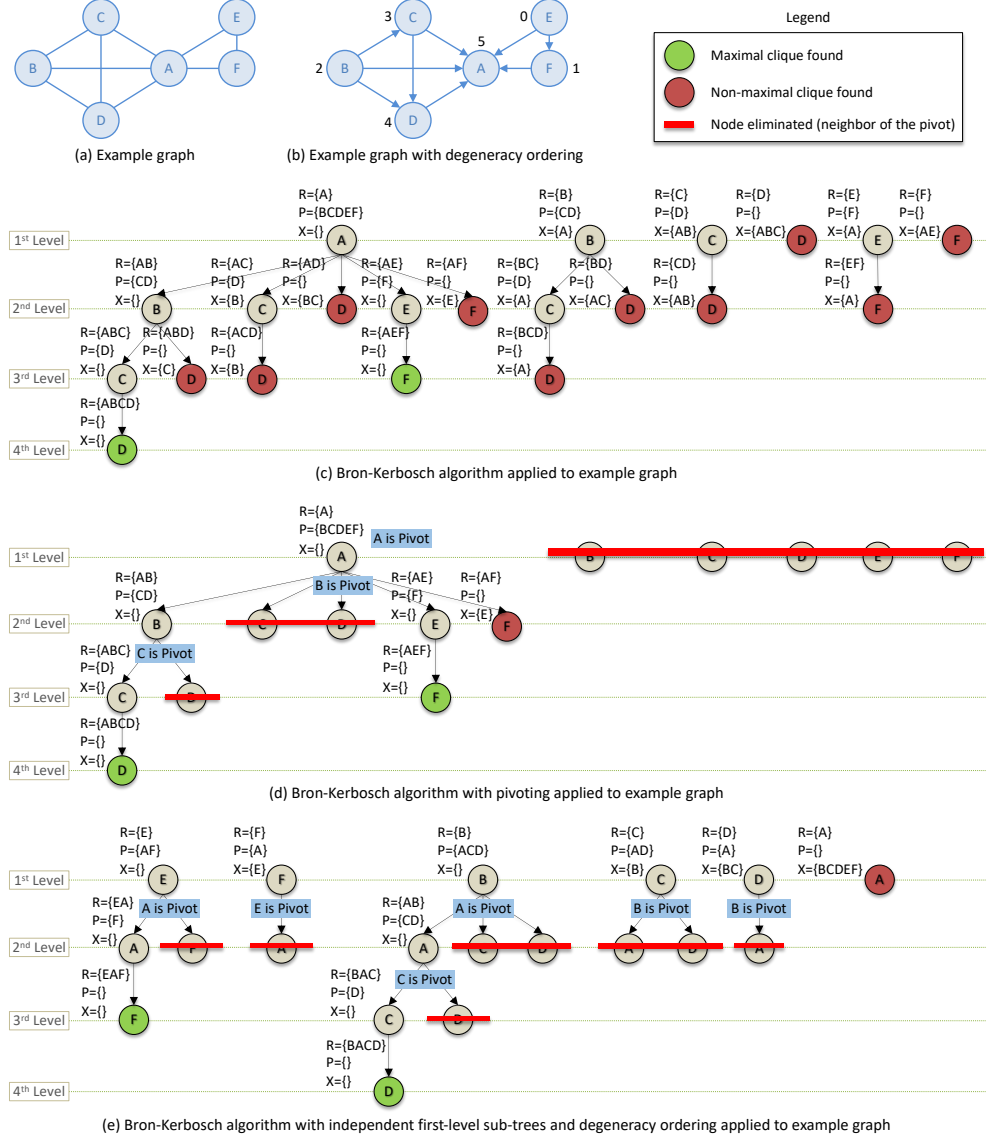


Figure 1. Bron-Kerbosch algorithm variants applied to example graph

Algorithm 2 Bron-Kerbosch algorithm with pivoting

```

1: procedure BRONKERBOSCHPIVOT( $G, R, P, X$ )
2:   if  $P$  and  $X$  are both empty then
3:      $R$  is a maximal clique
4:    $v_{pivot}$  = choose a vertex from  $P \cup X$ 
5:   for  $v \in (P - N(v_{pivot}))$  do
6:     BRONKERBOSCHPIVOT( $G, R \cup \{v\}, P \cap N(v), X \cap N(v)$ )
7:    $P = P - \{v\}$ 
8:    $X = X \cup \{v\}$ 

```

add non-neighbors of the pivot vertex to R . Therefore, there is no need to explore the pivot vertex's neighbors on line 5.

The pivot vertex can be any vertex, but is typically selected to have the largest number of common neighbors with the vertices in P in order to maximize the number of

branches that are excluded from the search. The original Bron-Kerbosch algorithm with pivoting selects the pivot vertex from P , but Tomita et al. [61] improve the pivot selection by considering all vertices in $P \cup X$.

2.4 Bron-Kerbosch with Other Optimizations

Eppstien et al. [22, 23] improve the Bron-Kerbosch algorithm with pivoting by introducing three key optimizations: independent first-level subtrees, degeneracy ordering, and induced subgraphs.

Independent First-level Subtrees. In Algorithms 1 and 2, the loop that iterates over the vertices in P has a loop-carried dependence for removing previously visited vertices from P and adding them to X . Eppstien et al. [22, 23] break this loop-carried dependence at the first level by having each

iteration independently remove all previous vertices from P and add them to X . The pseudocode for doing so is shown in Algorithm 3. In each iteration, P for vertex v_i is initialized by intersecting $N(v_i)$ with all the vertices that come after v_i (line 3), which removes all the neighbors of v_i that are visited on prior iterations. Similarly, X for vertex v_i is initialized by intersecting $N(v_i)$ with all the vertices that come before v_i (line 4), which removes all the neighbors of v_i that are visited on later iterations, keeping only those visited on prior iterations. The key advantage of breaking this loop-carried dependence is that each loop iteration, which represents a first-level subtree, can be treated as a unit of parallel work. For the second level onward, the algorithm simply calls the sequential BRONKERBOSCHPIVOT function (line 5).

Algorithm 3 Bron-Kerbosch algorithm with independent first-level subtrees

```

1: procedure BRONKERBOSCHINDEPENDENTFIRSTLEVEL( $G$ )
2:   for  $v_i \in V$  do
3:      $P = N(v_i) \cap \{v_{i+1}, v_{i+2}, \dots, v_{|V|-1}\}$ 
4:      $X = N(v_i) \cap \{v_0, v_1, \dots, v_{i-1}\}$ 
5:     BRONKERBOSCHPIVOT( $G, \{v_i\}, P, X$ )

```

Degeneracy Ordering. In Algorithm 3, the subtree for each vertex v_i only considers the vertices in P . Moreover, in Algorithm 2 (which is called by Algorithm 3 on line 5 to solve each subtree), several expensive set operations are performed with P such as $P - N(v_{pivot})$ (line 5) and $P \cap N(v)$ (line 6). Hence, the size of P directly impacts the size of the subtree traversed and the cost of the set operations performed by the traversal. Recall that P represents the neighbors of v_i that are ordered after v_i , and X represents the neighbors of v_i that are ordered before v_i . For an arbitrary graph, the sizes of P and X are $O(\Delta)$ where Δ denotes the maximum degree of the graph and can be quite large for real graphs. To place a tighter bound on the size of P , Eppstien et al. [22] propose to reorder vertices based on *degeneracy ordering* which minimizes the number of neighbors of any vertex that are ordered after that vertex. After degeneracy ordering, the maximum number of neighbors of any vertex that are ordered after that vertex is known as the degeneracy of the graph, and is denoted by d . The size of P thus becomes $O(d)$. For real graphs, d is typically much smaller than Δ (see Table 1).

The advantage of degeneracy ordering is that by placing a smaller bound on the sizes of the P sets, it places a smaller bound on the sizes of the subtrees traversed and the cost of the set operations performed with P . However, the size of the X sets remains $O(\Delta)$, and the practical sizes of the X sets increase since vertices are more likely to have their neighbors ordered before them. Hence, the trade-off of degeneracy ordering is that it makes the operations on the X sets, such as $X \cap N(v)$ (line 5 in Algorithm 2), more expensive.

In Figure 1(a), the first vertex A was also the vertex with the highest degree, which resulted in large subtrees being

visited for vertex A in Figures 1(c) and (d). The size of the P set for A was five which is the Δ of the graph. Figure 1(b) shows how the graph in Figure 1(a) can be reordered based on degeneracy ordering. In this figure, the graph is still intended to be undirected, but the edges are drawn with arrows from vertices earlier in the order to vertices later in the order. As shown in Figure 1(b), A is now the last vertex in the order and has no vertices ordered after it. Figure 1(e) shows how the example graph in Figure 1(a) can be processed using independent first-level subtrees and degeneracy ordering. It is clear that compared to Figures 1(c) and (d), Figure 1(e) has more independent subtrees that are each smaller in size, and its largest P set is also smaller than the largest P set in Figures 1(c) and (d). The trade-off is that its largest X set is larger than the largest X set in Figures 1(c) and (d).

Induced Subgraphs. In Algorithm 3, the subtree for each vertex v_i only needs to access information about the neighbors of v_i and their edges. It does not need to access the entire graph. Based on this observation, Eppstien et al. [22] propose to construct an induced subgraph for each subtree that only includes the information needed by that subtree. In particular, we observe that in Algorithm 2, three key operations are performed that access information from the graph. The first operation is $P - N(v_{pivot})$ (line 5). Since $v_{pivot} \in P \cup X$, this operation requires us to know the neighbors of any vertex in $P \cup X$ that are in P . The second operation is $P \cap N(v)$ (line 6). Since $v \in P$, this operation requires us to know the neighbors of any vertex in P that are also in P . The third operation is $X \cap N(v)$ (line 6). Since $v \in P$, this operation requires us to know the neighbors of any vertex in P that are in X . Overall, we need the edges connecting any vertex in $P \cup X$ with any vertex in P . Eppstien et al. [22] induce a subgraph that contains only this information, denoted by $H_{P,X}$. The key advantage of using an induced subgraph is that it removes irrelevant edges from the adjacency lists, making set operations on the adjacency lists smaller.

Without degeneracy ordering, the size of $P \cup X$ is $O(\Delta)$ and the size of P is $O(\Delta)$. Hence, the size of $H_{P,X}$ is $O(\Delta^2)$ which is prohibitively expensive to store for large graphs. However, after degeneracy ordering, the size of $P \cup X$ remains $O(\Delta)$ but the size of P is reduced to $O(d)$, which reduces the size of $H_{P,X}$ to $O(\Delta \cdot d)$. Since d is typically much smaller than Δ , another benefit of vertex ordering is that it makes it more feasible to construct and store the induced subgraph.

3 Parallel MCE on GPUs

3.1 Challenges and Implementation Overview

We propose a parallel implementation of MCE on GPUs based on the Bron-Kerbosch algorithm with pivoting, independent first-level subtrees, degeneracy ordering, and induced subgraphs. One of the main challenges for parallelizing the Bron-Kerbosch algorithm on GPUs is extracting a sufficient amount of parallelism to fully-utilize the hardware resources.

The majority of prior works [5, 35, 40, 69] do so by performing a breadth-first traversal of the search tree. Breadth-first search is highly amenable to parallelization because tree nodes at each level of the search tree can be processed in parallel. However, it does not scale well for large graphs because of the explosion in the number of search tree nodes that need to be tracked as the level gets deeper. To avoid this explosion, one work [36] performs a depth-first traversal on the CPU while offloading primitive operations to the GPU. However, this approach results in high communication overhead between the CPU and the GPU due to frequent kernel calls and data transfer operations.

To overcome these limitations, we propose to parallelize MCE on GPUs by assigning independent subtrees to different thread blocks and having each thread block perform a depth-first traversal of its subtree. Threads within the block collaborate to perform primitive operations such as set operations and finding the pivot vertex. This approach prevents the explosion in the number of search tree nodes that need to be tracked, and performs the entire traversal in a single kernel which eliminates CPU-GPU communication.

The parallelization approach of performing per-block depth-first traversals of independent subtrees has been applied by prior works to related problems such as k -clique counting [3] and subgraph matching [11]. To the best of our knowledge, our work is the first to apply this approach to MCE on GPUs. Moreover, prior works on related problems also apply other optimizations such as binary encoding of the induced subgraph [3] and partitioning work within a block at subwarp granularity [3]. In our work, we adopt these same optimizations as well. To the best of our knowledge, our work is the first to use induced subgraphs, binary encoding, and subwarp partitioning for parallelizing MCE on GPUs.

Directly applying these techniques to MCE is not straightforward because MCE has two key scalability challenges that are less of a concern in other related problems. The first challenge is that MCE has substantially higher load imbalance. In k -clique counting and subgraph matching, search trees have bounded depth depending on the size of the clique or pattern that is being searched for. Hence, the sizes of the subtrees that are assigned to different thread blocks are reasonably balanced. Moreover, prior work on k -clique counting [3] shows that extracting independent subtrees at the second level instead of the first level is sufficient to balance the load completely. In contrast, in MCE, the subtrees may be arbitrarily deep depending on the size of the maximal cliques they are exploring. Hence, MCE suffers from substantially higher load imbalance than other related problems, which requires more sophisticated load balancing techniques.

The second challenge is that MCE has a substantially higher memory footprint. Since MCE has potentially deeper subtrees, it needs to pre-allocate more stack space per thread block to support the depth-first traversal of these subtrees. Moreover, in k -clique counting, the traversal only needs to

track the equivalent of the R and P sets at each level of the tree, which are $O(d)$ in size, and the induced subgraphs only need to store the edges between vertices in P and other vertices also in P , which requires $O(d^2)$ space. In contrast, in MCE, to test for maximality, the traversal also needs to track the X set for each level of the tree, which is $O(\Delta)$ in size, and the induced subgraphs also need to store the edges between vertices in X and vertices in P , which requires $O(\Delta \cdot d)$ space. Since Δ is much larger than d , MCE has a substantially higher memory footprint than other related problems, which requires more sophisticated techniques for representing induced subgraphs and the X sets.

In the rest of this section, we describe our proposed approach for parallelizing MCE on GPUs, with a particular focus on unique aspects of our work, namely, how to mitigate load imbalance and how to efficiently represent induced subgraphs and the X sets at each level of the tree.

3.2 Independent Second-level Subtrees

One common approach to improving load balance on GPUs is to extract many more parallel tasks than the number of tasks that can be executed simultaneously by the hardware. Prior work on k -clique counting [3] shows that extracting independent subtrees at the second level instead of the first level is sufficient to balance the load completely for that problem. We apply the same technique to MCE.

Algorithm 4 shows the pseudocode for extracting independent second-level subtrees. Instead of iterating over vertices in V , we iterate over edges $\{v_i, v_j\}$ in E (line 2). For each edge, P is initialized to the common neighbors of v_i and v_j that are ordered after both vertices (line 3). On the other hand, X is initialized to the common neighbors of v_i and v_j that are ordered before the later of the two vertices (line 4).

Algorithm 4 Bron-Kerbosch algorithm with independent second-level subtrees

```

1: procedure BRONKERBOSCHINDEPENDENTSECONDLEVEL( $G$ )
2:   for  $\{v_i, v_j\} \in E$  do
3:      $P = N(v_i) \cap N(v_j) \cap \{v_{\max(i,j)+1}, \dots, v_{|V|-1}\}$ 
4:      $X = N(v_i) \cap N(v_j) \cap \{v_0, \dots, v_{\max(i,j)-1}\}$ 
5:     BRONKERBOSCHPIVOT( $G, \{v_i, v_j\}, P, X$ )

```

The advantage of extracting subtrees at the second level instead of the first level is that it provides more parallel tasks to assist with load balancing. It also results in smaller induced subgraphs since the P sets at the second level are smaller than those at the first level. The disadvantage is that more induced subgraphs need to be constructed overall, and their construction cost is amortized across smaller subtrees.

We evaluate the trade-off between extracting subtrees at the first or second level throughout Section 4. We observe that although extracting second-level subtrees partially reduces load imbalance, the imbalance remains high for many

graphs. This observation motivates us to propose another optimization for mitigating load imbalance in MCE.

3.3 Dynamic Load Balancing with a Worker List

One approach to alleviate load imbalance on GPUs is by using a *worklist*. Thread blocks with large tasks can add subtasks to the worklist, and thread blocks that complete their tasks can remove subtasks from the worklist. However, in MCE, the data needed to represent a subtask is large, consisting of the R , P , X , the current level, and a reference to the induced subgraph. The large size of the subtask data makes using a worklist inefficient for MCE for two reasons. The first reason is that a large amount of memory would be needed to store the worklist entries, which would place high pressure on the already constrained memory capacity. The second reason is that adding and removing subtasks from the worklist would incur high overhead, so there would be a high penalty when a block adds work to a worklist and there are no idle blocks actually needing any work.

To avoid the limitations of using a worklist, we instead propose to use a *worker list* for dynamic load balancing. The worker list holds IDs of thread blocks that are idle because they have completed their previous tasks. A thread block that completes its task adds its ID to the worker list to indicate that it can receive subtasks from other blocks. We call this block a *receiver* block. On the other hand, a thread block working on a large task periodically checks the worker list to see if there are any receiver blocks waiting. We call this block a *donor* block. If a donor block finds a receiver block in the worker list, the donor block removes the receiver block and gives it a subtask to work on. The computation terminates when all blocks have added themselves to the worker list and there are no more executing donor blocks.

We incorporate our proposed worker list technique into our parallel MCE implementation as follows. We start by launching as many thread blocks as the maximum number that can run on the GPU simultaneously. These blocks execute in two phases. In the first phase, each block atomically increments a shared counter to reserve an independent first- or second-level subtree, and traverses that subtree. If the block completes the subtree, it atomically increments the counter again to obtain another subtree. This process continues until all the independent subtrees have been depleted, after which the second phase begins. Note that there is no global synchronization needed between the two phases. Donor blocks that are still executing their subtrees from the first phase know when the second phase has been reached by checking the shared counter every time they branch.

In the second phase, blocks that finish traversing their subtrees add themselves to the worker list and sleep by spinning on a flag with exponential back-off. The worker list is implemented as a multi-producer multi-consumer queue using a circular buffer. The buffer cannot overflow because the number of thread blocks is fixed. Donor blocks that have

not finished traversing their subtrees check the worker list upon visiting a new branch. If a donor finds a receiver in the worker list, the donor atomically removes the receiver's ID from the worker list, offloads the new branch to the receiver by initializing the receiver's data structures, and wakes the receiver up by setting its flag. We use CUDA atomic objects from `libcu++` and the release-acquire model to guarantee that data written by the donor is visible to the receiver.

In some cases, the benefit of a donor block offloading a branch to a receiver block is not worth the overhead. To avoid these unprofitable cases, we only have a donor block check the worker list and offload a branch if two conditions hold. The first condition is that the branch to be offloaded should not be small, otherwise the overhead of offloading the branch to the receiver may be higher than the cost of visiting the branch. To ensure that the branch is not small, we require that $|P| \geq 10$ for the root node of the branch, however we note that performance is not very sensitive to the choice of this threshold. The second condition is that the donor block should have a substantial amount of other work to do after offloading the branch, because it does not make sense for the donor to offload a branch, then finish traversing its subtree shortly after and start seeking work from other donors. To ensure that the donor has a substantial amount of other work, we only offload a branch if there are other branches at the same level *and* other branches in previous levels that have not yet been explored.

We evaluate the advantage of using a worker list in Sections 4.3 and 4.4, including its importance when scaling to multiple GPUs.

3.4 Partial Induced Subgraphs

Recall from Section 2.4 that one common optimization to reduce the size of adjacency lists and intersection operations is to construct, for each independent subtree, an induced subgraph with vertices and edges relevant to that subtree. Prior works that implement MCE on GPUs [5, 35, 36, 40, 69] do not apply this optimization because they do not perform depth-first traversal of independent subtrees entirely on the GPU. To the best of our knowledge, our work is the first to use induced subgraphs for MCE on GPUs.

As mentioned in Section 3.1, the induced subgraphs in MCE contain the edges between the vertices in P and the vertices in $P \cup X$, which makes the size of the induced subgraph $O(\Delta \cdot d)$. Since Δ can be large, these induces subgraphs are expensive to construct and store. To address this challenge, we propose to represent the induced subgraph using two alternatives: full or partial. For full induced subgraphs, we construct binary-encoded induced subgraphs containing all the edges between P and $P \cup X$. For partial induced subgraphs, we construct binary-encoded induced subgraphs with only the edges between vertices P and other vertices also in P , and use the original graph to look up edges between vertices in P and vertices in X . The original graph

is stored using CSR when first-level subtrees are used, and CSR+COO when second-level subtrees are used.

The advantage of using full induced subgraphs is that it makes set operations on X faster by using bit-wise operations. The advantage of using partial induced subgraphs is that it avoids the high latency of constructing large induced subgraphs and the high memory capacity required for storing it. We evaluate these trade-offs in Section 4.5.

3.5 Compact Representation of the X Sets

Recall from Section 3.1 that MCE puts higher pressure on the memory capacity than other related problems because of the need to represent X at each level of a subtree to test for maximality. A subtree can have up to d levels, and the size of X is $O(\Delta)$. Therefore, a naive representation of the X sets would require $O(\Delta \cdot d)$ memory per subtree. Hence, the memory needed to represent the X sets can easily limit the number of subtrees that can be traversed in parallel.

To design an efficient representation of X , we first make the following observations. In Algorithm 2, the two operations that modify X as the tree is traversed are $X \cap N(v)$ (line 6) and $X \cup \{v\}$ (line 8), where $v \in P$. The first operation, $X \cap N(v)$, can only remove vertices from X . The second operation, $X \cup \{v\}$, adds vertices to X but these vertices can only come from P . Based on this observation, we divide the representation of X into two parts: X_P and X_X .

X_P represents the vertices in X that are part of the original P set at the root node of the subtree. These vertices may be added by the $X \cup \{v\}$ operation or removed by the $X \cap N(v)$ operation. Hence, X_P may grow or shrink as we descend to deeper levels of the subtree. However, X_P may not exceed the size of P which is $O(d)$. For this reason, X_P is binary encoded for fast set operations on it, and a different copy of X_P is stored for each level of the tree.

On the other hand, X_X represents the vertices in X that were part of the original X set at the root node of the subtree. X_X may contain any vertex in the original X which makes its size $O(\Delta)$. However, since the vertices in the original X cannot be part of any P set in the subtree, the vertices in X_X may only be removed by the $X \cap N(v)$ operation as we descend to deeper levels of the tree. Since X_X only shrinks as we descend down the tree, we do not need to store a separate copy of X_X for each level. Instead, we store a single copy of X_X for all levels and an index for each level that points to where the X_X vertices end for that level.

Figure 2 shows an example of how X_X is represented and updated as we descend down the tree. In this example, as we descend from Level 0 to Level 1, the vertices that remain in X in Level 1 are moved to the earlier part of the array and the vertices that are removed are moved to the later part of the array. To move the vertices, we implement an out-of-place partition operation where each thread moves one value after atomically incrementing a bin counter. We also tried the in-place partition operation in CUB [47] but it

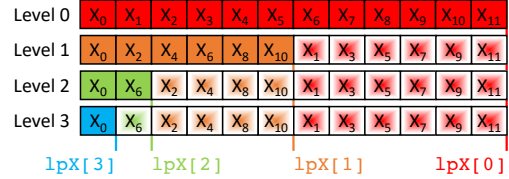


Figure 2. Using a single array to represent X_X across levels

did not yield better performance. After moving the vertices, a level pointer array $1pX$ is updated such that $1pX[1]$ points to where the vertices in Level 1 end. The same process is repeated as we descend to deeper levels. To go back up to a previous level, nothing needs to be done since all the vertices for the previous level have stayed within the previous level's $1pX$ value and only their order has changed.

By storing only a single copy of X_X for all levels and different copies of X_P for each level, the memory needed for representing X for all levels becomes $O(\Delta + d^2)$ which is much smaller than $O(\Delta \cdot d)$. This compact representation is crucial for scalable acceleration of MCE on GPUs (and any other memory constrained system) and is used in all our implementations.

Finally, we note that if a partial induced subgraph is used instead of a full induced subgraph (see Section 3.4), then the pivot is only selected from $X_P \cup P$. The reason is that finding a pivot vertex from X_X is expensive if the adjacency lists of the vertices in X_X are not binary encoded.

4 Evaluation

4.1 Methodology

Evaluation Platforms. We evaluate our GPU implementations on two platforms. The first platform has four 32GB NVIDIA V100 GPUs attached to an Intel Xeon Gold 6230 CPU and is used for both single- and multi-GPU evaluation. The second platform has a 40GB NVIDIA A100 GPU attached to an AMD EPYC 7702 CPU and is used for the single-GPU evaluation only.

CPU Baselines. To the best of our knowledge, the work of Blanuša et al. [7] is the state-of-the-art parallel CPU implementation of MCE. We compare the performance of our GPU implementations with the best execution times reported by Blanuša et al. which are obtained using a dual-socket Intel Xeon Skylake platform with 48 cores (96 threads) and 360 GB of main memory. For completeness, we also execute their implementation on our dual-socket Intel Xeon Gold 6230 Cascade Lake CPU with 40 cores (80 threads) and 512GB of main memory and report those results as well.

Datasets We evaluate using the same graph datasets used by Blanuša et al. [7] which are shown in Table 1.

Reporting of Measurements. The execution times reported by Blanuša et al. [7] include the time spent on counting maximal cliques and exclude the time spent on reading the graph from disk. For fair comparison, we follow the same strategy. We also include the time spent on pre-processing

Table 1. Graphs used for evaluation and comparison of execution time with the state-of-the-art parallel CPU implementation

Graph	V	E	Max degree (Δ)	Degeneracy (d)	# of maximal cliques	Avg maximal clique size	Max clique size	Parallel CPU time (s)		GPU time (s)		GPU speedup over Skylake with 96 threads	
								Cascade Lake with 80 threads	Skylake with 96 threads [7]	V100	A100	V100	A100
wiki-talk [39]	2,394,385	4,659,565	100,029	131	86,333,306	13.37	26	4.57	4	1.39	1.38	2.89	2.91
as-skitter [39]	1,696,415	11,095,298	35,455	111	37,322,355	19.91	67	3.74	3	0.81	0.79	3.70	3.82
sofb-b-anon [53]	2,937,613	20,959,854	4,356	63	27,593,398	5.24	24	2.38	2	0.56	0.45	3.60	4.42
soc-pokec [39]	1,632,804	22,301,964	14,854	47	19,376,873	3.67	29	1.45	1	0.38	0.36	2.65	2.78
wiki-topcats [39]	1,791,489	25,444,207	238,342	99	27,229,873	4.46	39	2.09	2	0.83	0.87	2.42	2.30
soc-livejournal [53]	4,033,138	27,933,062	2,651	213	38,413,665	29.97	214	5.45	5	0.81	0.76	6.21	6.57
soc-orkut [53]	3,072,442	117,185,083	33,313	253	2,269,631,973	20.24	51	110.61	93	25.23	17.82	3.69	5.22
soc-sinaweibo [53]	58,655,850	261,321,033	278,489	193	1,117,416,174	18.43	44	67.78	54	16.40	13.60	3.29	3.97
aff-orkut [53]	8,730,858	327,036,486	318,268	471	417,032,363	2.53	6	138.89	147	14.40	8.82	10.21	16.67
clueweb09-50m [53]	428,136,613	446,766,953	308,477	192	1,001,323,679	15.21	56	99.29	90	14.90	10.03	6.04	8.97
wiki-link [53]	27,154,799	543,183,611	4,271,341	1,120	568,730,123	4.51	428	112.14	109	34.82	32.23	3.13	3.38
soc-friendster [53]	65,608,367	1,806,067,135	5,214	304	3,364,773,700	6.88	129	406.33	380	64.50	39.59	5.89	9.60

the graph to apply degeneracy ordering. Unless otherwise specified, we report the time achieved with the worker list enabled, and with the best combination of using independent first- or second-level subtrees and using partial or full induced subgraphs.

No GPU Baselines. We do not compare to any GPU baselines for two reasons. The first reason is that upon comparing the execution times reported in various prior works, we found that the work of Blanuša et al. [7] outperforms all prior GPU implementations of MCE. Therefore, comparing with Blanuša et al. subsumes comparing with prior GPU implementations. The second reason is that prior GPU implementations have difficulty scaling to graphs with a large number of maximal cliques because of the memory scalability limitations of breadth-first traversal, as discussed in Section 3.1. For example, none of these implementations evaluate on soc-orkut and soc-friendster, the two graphs with the largest number of maximal cliques as shown in Table 1.

4.2 Performance

Table 1 compares the execution time of our single-GPU implementation with the state-of-the-art parallel CPU implementation [7]. We observe that our GPU implementation consistently and significantly outperforms the parallel CPU implementation for all graphs. The geometric mean speedup of our GPU implementation over the parallel CPU implementation is $4.1\times$ (up to $10.2\times$) for the V100 GPU and $4.9\times$ (up to $16.7\times$) for the A100 GPU. These results show the effectiveness of GPUs at accelerating MCE, despite the challenges of GPUs being more sensitive to load imbalance and having more constrained memory capacity.

4.3 Load Balance

Figure 3 compares the distribution of load across SMs when different combinations of optimizations are applied on an A100 GPU. The load of an SM is measured as the maximum number of tree nodes visited by any block on that SM (recall that we launch exactly the maximum number of concurrent blocks that can execute and reuse these blocks to process different subtrees). Based on these results, we make three key observations.

Table 2. Number of donations with a worker list on A100

Graph	L1	L2	Graph	L1	L2
wiki-talk	1,436,113	74,268	soc-orkut	9,728,983	2,438,166
as-skitter	625,508	74,703	soc-sinaweibo	11,119,926	1,164,829
sofb-b-anon	170	0	aff-orkut	0	0
soc-pokec	0	0	clueweb09-50m	890,122	49,799
wiki-topcats	2,128	28	wiki-link	2,997	99
soc-livejournal	341,721	105,270	soc-friendster	1,615,437	358,499

The first observation is that when no worker list is used (No WL), using independent second-level subtrees (L2) instead of independent first-level subtrees (L1) substantially reduces load imbalance. This observation is consistent with prior work on related problems [3]. However, we note that in the case of MCE, even after L2 trees are used, the imbalance is still high for some graphs. The average across benchmarks of the maximum load across thread blocks is $2.28\times$ the average load when using L1 trees and $1.63\times$ the average load when using L2 trees, which is a $1.40\times$ decrease in imbalance.

The second observation is that using a worker list (WL) substantially reduces load imbalance compared to not using a worker list. To further study the effectiveness of the worker list, Table 2 shows the number of donations performed for each graph on A100. It is clear that the graphs with a large number of donations are also the ones with high imbalance in Figure 3 that benefit from using the worker list. These results show the effectiveness of our proposed worker list approach at reducing load imbalance of MCE on GPUs.

The third observation is that when a worker list is used, there is little difference in load imbalance between using L1 trees and L2 trees in most cases. The average across benchmarks of the maximum load across thread blocks is $1.17\times$ the average load when using L1 trees and $1.11\times$ the average load when using L2 trees, which is only a $1.05\times$ decrease in imbalance. This observation shows that our proposed worker list approach obviates the need to use L2 trees for the purpose of load balancing in most cases. Still, using L2 trees may have other benefits such as smaller induced subgraphs and shorter set operations. We revisit this point in Section 4.5.

4.4 Scalability to Multiple GPUs

Figure 4 shows the strong scaling of our GPU implementation across multiple V100 GPUs when different combinations of optimizations are applied. In the multi-GPU implementation,

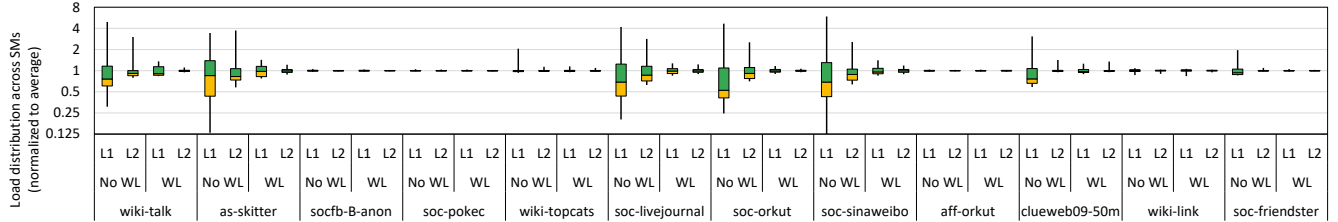


Figure 3. Load distribution across streaming multiprocessors (SMs) for different combinations of optimizations on A100

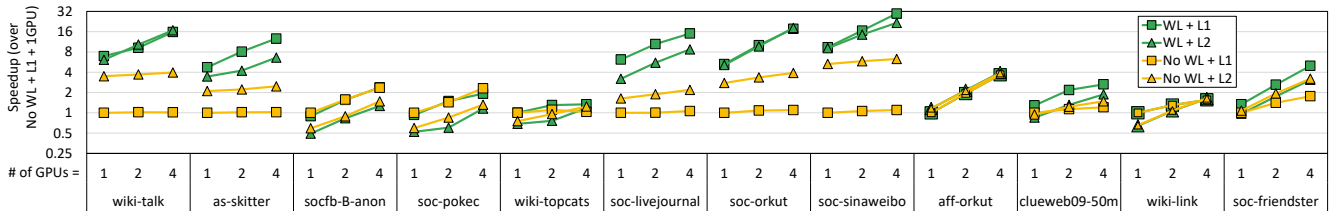


Figure 4. Strong scaling with respect to the number of GPUs for different combinations of optimizations on V100s

L1 or L2 trees are distributed across GPUs in a round-robin scheme and each GPU maintains its own private worker list. We also experimented with using an inter-GPU shared worker list, however its overhead was not worth its benefit. Currently, our implementation supports scaling to multiple GPUs within a single node, however, scaling to multiple GPU nodes is the subject of future work.

Based on the results in Figure 4, we make three key observations. The first observation is that in most cases, on a single GPU, the implementations that use a worker list substantially outperform those that do not use a worker list. This observation shows the effectiveness of our proposed worker list approach at improving performance by reducing load imbalance.

The second observation is that in most cases, as we scale to multiple GPUs, the WL implementation scales well whereas the No WL implementation scales poorly. This observation shows that scaling to multiple GPUs exacerbates the load imbalance challenge of MCE, and that our proposed worker list approach is effective at overcoming this scalability challenge.

The third observation is that in most cases, using L2 trees instead of L1 trees has better performance and scalability when no worker list is used, but does not significantly improve performance and scalability when a worker list is used and may even degrade performance. This observation reiterates the observation in Section 4.3 that our proposed worker list approach obviates the need to use L2 trees for the purpose of load balancing.

4.5 Breakdown of Execution Time

Figure 5 shows the breakdown of execution time when different combinations of optimizations are applied on A100. The breakdowns are obtained by using SM clocks to get the number of cycles spent by each thread block on each activity.

When comparing the use of L1 trees with L2 trees, we make two key observations. The first observation is that in

most cases, the fraction of time spent on constructing the induced subgraph is larger for L2 trees. The reason is that using L2 trees extracts more subtrees that are each smaller in size, so more induced subgraphs are generated and the cost of generating them is amortized across fewer tree node traversals. The second observation is that in most cases, the fraction of time spent on set operations (such as intersections) is smaller for L2 trees. The reason is that using L2 trees results in smaller induced subgraphs, hence smaller sets to operate on. Nevertheless, the benefit of faster set operations does not overcome the increased overhead of constructing induced subgraphs, so we find that using L1 trees outperforms using L2 trees in the majority of cases. On average, using L1 trees is 1.2 \times (geometric mean) faster than using L2 trees. Note that in prior work on related problems, L2 trees were more effective in most cases because of their load balancing benefits. However, since these benefits are obviated by the worker list (see Sections 4.3 and 4.4), the benefits of L1 trees become more pronounced.

When comparing the use of partial induced subgraphs (IP, i.e., induced on P only) and full induced subgraphs (IPX, i.e., induced on P and X), we make three key observations. The first observation is that in most cases, the fraction of time spent on constructing induced subgraphs is larger for IPX. The reason is that the induced subgraphs in IPX are larger than the induced subgraphs in IP, thereby taking longer to construct. The second observation is that in most cases, the fraction of time spent on pivoting is larger for IPX. The reason is that in IPX, we consider pivots from $X \cup P$, whereas in IP, we only consider pivots in $X_P \cup P$ and do not consider pivots from X_X . As a result, we spend less time on pivoting in IP, however, we may not find the best possible pivot. The third observation is that in most cases, the fraction of time spent on set operations is smaller for IPX. The reason is that including the edges between P and X vertices in the

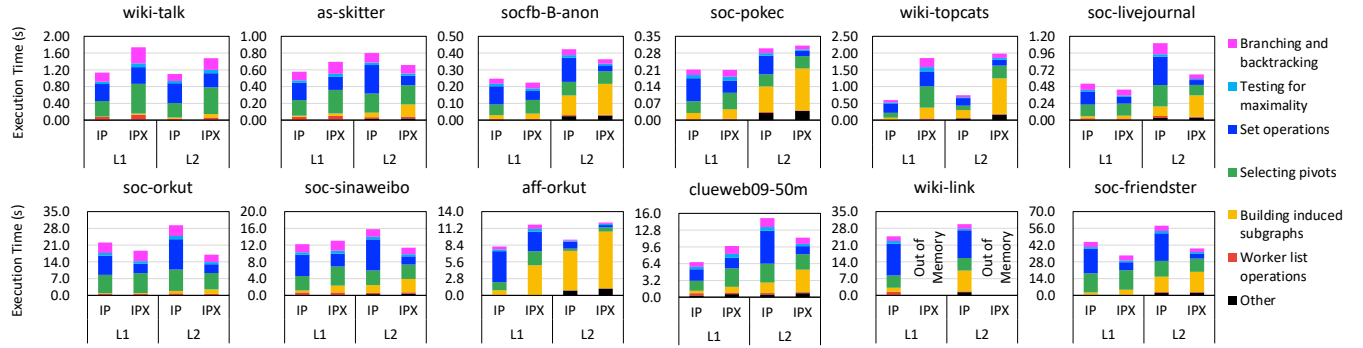


Figure 5. Breakdown and comparison of execution time for different combinations of optimizations on A100

Table 3. Comparing heuristic (underlined) and optimal (bold) selection of optimization combinations on A100

Graph	Δ/d	Execution time (s)				Heuristic slowdown
		L1 + IP	L1 + IPX	L2 + IP	L2 + IPX	
wiki-talk	763.58	<u>1.14</u>	1.74	1.10	1.48	1.03
as-skitter	319.41	0.58	0.70	0.80	0.66	1.00
socfb-B-anon	69.14	0.25	0.22	0.42	0.36	1.00
soc-pokec	316.64	0.21	0.21	0.30	0.31	1.00
wiki-topcats	2,407.49	0.60	1.85	0.74	1.99	1.00
soc-livejournal	12.45	0.52	0.44	1.10	0.65	1.00
soc-orkut	131.67	22.10	<u>18.68</u>	29.29	16.98	1.10
soc-sinaweibo	1,442.95	12.20	13.05	15.80	11.39	1.07
aff-orkut	675.73	8.16	11.82	9.31	12.18	1.00
clueweb09-50m	1,606.65	6.70	9.77	15.10	11.35	1.00
wiki-link	3,813.70	24.67	-	29.76	-	1.00
soc-friendster	17.15	44.64	33.41	58.16	39.17	1.00
Geomean						1.02

induced subgraphs makes set operations on the X sets less costly. This trade-off between the time spent on constructing induced subgraphs, the time spent on pivoting, and the time spent on performing set operations makes each approach perform better on different datasets. Overall, IP performs better in six cases whereas IPX performs better in six cases.

To select the best combination of optimizations, we recommend the following heuristic. First, L1 trees should always be selected instead of L2 trees. Second, IP should be selected when $\Delta/d > 200$, and IPX should be selected otherwise. The intuition is that IPX requires $O(\Delta \cdot d)$ space for each induced subgraph and IP requires only $O(d^2)$ space, so Δ/d represents how much more space IPX requires compared to IP. If this value is too high (IPX requires too much more space), it is better to select IP, otherwise it is better to select IPX. Table 3 shows that this heuristic selects the best combination in the majority of cases, with a geometric mean slowdown of $1.02\times$ (up to $1.10\times$) from selecting incorrectly.

Finally, we make one additional overall observation that the fraction of time spent adding to and removing from the worker list is small. This observation shows that the substantial load balancing benefits that the worker list provides come with a low performance overhead. Furthermore, the fraction of time spent performing worker list operations in Figure 5 tends to be larger for graphs where a large number of donations is performed according to Table 2.

5 Related Work

MCE has been extensively studied on CPUs [9, 12, 22, 61, 72] and many attempts to parallelize it on the CPU have been made [7, 13, 17, 18, 57, 73]. To the best of our knowledge, the work of Blanuša et al. [7] is the state-of-the-art parallel CPU implementation of MCE, and its reported performance is the highest among all prior CPU (and GPU) implementations. Our work targets accelerating MCE on GPUs. We compare the performance of our work to that of Blanuša et al. [7] in Section 4. Many works have parallelized MCE on GPUs [5, 35, 36, 40, 69]. We compare our approach to these works in depth in Section 3.1.

k -clique enumeration has been extensively studied on CPUs [14, 16, 24, 26, 41, 43, 58] and GPUs [3]. Triangle counting, which is a special case of k -clique counting, has also been extensively studied on CPUs [2, 33, 37, 48, 60] and the GPUs [4, 6, 28, 29, 34, 45, 49, 50, 64, 67]. Our work uses similar techniques to those used in prior GPU work on k -clique counting [3], namely per-block depth-first traversal, binary encoding of induced sub-graphs, and sub-warp partitioning. However, as discussed in Section 3.1, MCE imposes unique challenges that we overcome with additional techniques such as the worker list, partial induced sub-graphs, and compact representation of excluded vertex sets.

Generalized graph pattern matching has also been extensively studied on CPUs [1, 20, 52, 56, 68] and GPUs [10, 11, 31, 32, 42, 62, 65, 66, 74]. Cliques are special cases of patterns that graph pattern matching works aim to find. While graph pattern matching algorithms perform similar tree traversals to those in MCE, their general nature makes them more difficult to scale. For example, using induced sub-graphs in graph pattern matching would require $O(\Delta^2)$ space, which causes most of these works to avoid such an optimization.

6 Conclusion

We present a GPU solution for accelerating maximal clique enumeration that assigns independent sub-trees to different thread blocks and has each thread block perform a depth-first traversal of its sub-tree. We propose a worker list for dynamic load balancing to mitigate the high imbalance in the

MCE search tree. We propose partial induced sub-graphs and a compact representation of excluded vertex sets to regulate memory consumption. We also apply various optimizations used in prior works such as binary encoding of the induced sub-graph and partitioning work at sub-warp granularity. Our evaluation shows that our GPU implementation substantially outperforms the state-of-the-art parallel CPU implementation, which outperforms prior GPU implementations.

References

[1] Nesreen K Ahmed, Jennifer Neville, Ryan A Rossi, Nick G Duffield, and Theodore L Willke. 2017. Graphlet decomposition: Framework, algorithms, and applications. *Knowledge and Information Systems* 50, 3 (2017), 689–722.

[2] Mohammad Al Hasan and Vachik S Dave. 2018. Triangle counting in large networks: a review. *Wiley Interdisciplinary Reviews: Data Mining and Knowledge Discovery* 8, 2 (2018), e1226.

[3] Mohammad Almasri, Izzat El Hajj, Rakesh Nagi, Jinjun Xiong, and Wen mei Hwu. 2021. Parallel K-Clique Counting on GPUs. *arXiv preprint arXiv:2104.13209* (2021).

[4] Mohammad Almasri, Neo Vasudeva, Rakesh Nagi, Jinjun Xiong, and Wen-Mei Hwu. 2021. HyKernel: A Hybrid Selection of One/Two-Phase Kernels for Triangle Counting on GPUs. In *2021 IEEE High Performance Extreme Computing Conference (HPEC)*. IEEE, 1–7.

[5] Tariq Alusaifeer, Sheela Ramanan, Christopher J Henry, and James Peters. 2013. GPU implementation of MCE approach to finding near neighbourhoods. In *International Conference on Rough Sets and Knowledge Technology*. Springer, 251–262.

[6] Mauro Bisson and Massimiliano Fatica. 2018. Update on static graph challenge on GPU. In *2018 IEEE High Performance extreme Computing Conference (HPEC)*. IEEE, 1–8.

[7] Jovan Blanuša, Radu Stoica, Paolo Inen, and Kubilay Atasu. 2020. Manycore clique enumeration with fast set intersections. *Proceedings of the VLDB Endowment* 13, 12 (2020), 2676–2690.

[8] Vladimir Boginski, Sergiy Butenko, and Panos M Pardalos. 2005. Statistical analysis of financial networks. *Computational statistics & data analysis* 48, 2 (2005), 431–443.

[9] Coen Bron and Joep Kerbosch. 1973. Algorithm 457: finding all cliques of an undirected graph. *Commun. ACM* 16, 9 (1973), 575–577.

[10] Xuhao Chen, Roshan Dathathri, Gurbinder Gill, and Keshav Pingali. 2020. Pangolin: an efficient and flexible graph mining system on CPU and GPU. *Proceedings of the VLDB Endowment* 13, 10 (2020), 1190–1205.

[11] Xuhao Chen and Arvind Satyanarayanan. 2021. Efficient and Scalable Graph Pattern Mining on GPUs. *arXiv preprint arXiv:2112.09761* (2021).

[12] James Cheng, Yiping Ke, Ada Wai-Chee Fu, Jeffrey Xu Yu, and Linhong Zhu. 2011. Finding maximal cliques in massive networks. *ACM Transactions on Database Systems (TODS)* 36, 4 (2011), 1–34.

[13] James Cheng, Linhong Zhu, Yiping Ke, and Shumo Chu. 2012. Fast algorithms for maximal clique enumeration with limited memory. In *Proceedings of the 18th ACM SIGKDD international conference on Knowledge discovery and data mining*. 1240–1248.

[14] Norishige Chiba and Takao Nishizeki. 1985. Arboricity and subgraph listing algorithms. *SIAM Journal on computing* 14, 1 (1985), 210–223.

[15] Hon Nian Chua, Kang Ning, Wing-Kin Sung, Hon Wai Leong, and Limsoon Wong. 2007. Using indirect protein-protein interactions for protein complex prediction. In *Computational Systems Bioinformatics: (Volume 6)*. World Scientific, 97–109.

[16] Maximilien Danisch, Oana Balalau, and Mauro Sozio. 2018. Listing k-cliques in sparse real-world graphs. In *Proceedings of the 2018 World Wide Web Conference*. 589–598.

[17] Apurba Das, Seyed-Vahid Sanei-Mehri, and Srikanta Tirthapura. 2020. Shared-memory parallel maximal clique enumeration from static and dynamic graphs. *ACM Transactions on Parallel Computing (TOPC)* 7, 1 (2020), 1–28.

[18] Naga Shailaja Dasari, Ranjan Desh, and Zubair M. 2014. pbitMCE: A bit-based approach for maximal clique enumeration on multicore processors. In *2014 20th IEEE International Conference on Parallel and Distributed Systems (ICPADS)*. 478–485. <https://doi.org/10.1109/PADSW.2014.7097844>

[19] Imre Derényi, Gergely Palla, and Tamás Vicsek. 2005. Clique percolation in random networks. *Physical review letters* 94, 16 (2005), 160202.

[20] Ethan R Elenberg, Karthikeyan Shanmugam, Michael Borokhovich, and Alexandros G Dimakis. 2016. Distributed estimation of graph 4-profiles. In *Proceedings of the 25th International Conference on World Wide Web*. 483–493.

[21] Abbasali Emamjomeh, Elham Saboori Robat, Javad Zahiri, Mahmood Solouki, and Pegah Khosravi. 2017. Gene co-expression network reconstruction: a review on computational methods for inferring functional information from plant-based expression data. *Plant biotechnology reports* 11, 2 (2017), 71–86.

[22] David Eppstein, Maarten Löffler, and Darren Strash. 2010. Listing all maximal cliques in sparse graphs in near-optimal time. In *International Symposium on Algorithms and Computation*. Springer, 403–414.

[23] David Eppstein, Maarten Löffler, and Darren Strash. 2013. Listing all maximal cliques in large sparse real-world graphs. *Journal of Experimental Algorithms (JEA)* 18 (2013), 3–1.

[24] Irene Finocchi, Marco Finocchi, and Emanuele G Fusco. 2015. Clique counting in mapreduce: Algorithms and experiments. *Journal of Experimental Algorithms (JEA)* 20 (2015), 1–20.

[25] Wei Gao, Kam-Fai Wong, Yunqing Xia, and Ruifeng Xu. 2006. Clique percolation method for finding naturally cohesive and overlapping document clusters. In *International Conference on Computer Processing of Oriental Languages*. Springer, 97–108.

[26] Lukas Gianiuzzi, Maciej Besta, Yannick Schaffner, and Torsten Hoefer. 2021. Parallel Algorithms for Finding Large Cliques in Sparse Graphs. In *Proceedings of the 33rd ACM Symposium on Parallelism in Algorithms and Architectures*. 243–253.

[27] Felipe Glaria, Cecilia Hernández, Susana Ladra, Gonzalo Navarro, and Lilian Salinas. 2021. Compact structure for sparse undirected graphs based on a clique graph partition. *Information Sciences* 544 (2021), 485–499.

[28] Oded Green, Pavan Yalamanchili, and Lluís-Miquel Munguía. 2014. Fast triangle counting on the GPU. In *Proceedings of the 4th Workshop on Irregular Applications: Architectures and Algorithms*. 1–8.

[29] Oded Green, Pavan Yalamanchili, and Lluís-Miquel Munguía. 2014. Fast Triangle Counting on the GPU. In *Proceedings of the 4th Workshop on Irregular Applications: Architectures and Algorithms* (New Orleans, Louisiana) (IA³ '14). IEEE Press, 1–8.

[30] Enrico Gregori, Luciano Lenzini, and Simone Mainardi. 2012. Parallel k-clique community detection on large-scale networks. *IEEE Transactions on Parallel and Distributed Systems* 24, 8 (2012), 1651–1660.

[31] Wentian Guo, Yuchen Li, Mo Sha, Bingsheng He, Xiaokui Xiao, and Kian-Lee Tan. 2020. GPU-accelerated subgraph enumeration on partitioned graphs. In *Proceedings of the 2020 ACM SIGMOD International Conference on Management of Data*. 1067–1082.

[32] Wentian Guo, Yuchen Li, and Kian-Lee Tan. 2020. Exploiting Reuse for GPU Subgraph Enumeration. *IEEE Transactions on Knowledge and Data Engineering* (2020).

[33] Mahantesh Halappanavar and Sayan Ghosh. 2020. *TriC: Distributed-memory Triangle Counting by Exploiting the Graph Structure*. Technical Report. Pacific Northwest National Lab.(PNNL), Richland, WA (United States).

[34] Yang Hu, Hang Liu, and H Howie Huang. 2018. High-performance triangle counting on GPUs. In *2018 IEEE High Performance extreme Computing Conference (HPEC)*. IEEE, 1–5.

[35] PB Jayaraj, K Rahamathulla, and G Gopakumar. 2016. A GPU based maximum common subgraph algorithm for drug discovery applications. In *2016 IEEE international parallel and distributed processing symposium workshops (IPDPSW)*. IEEE, 580–588.

[36] John Jenkins, Isha Arkatkar, John D Owens, Alok Choudhary, and Nagiza F Samatova. 2011. Lessons learned from exploring the backtracking paradigm on the GPU. In *European Conference on Parallel Processing*. Springer, 425–437.

[37] Mihail N Kolountzakis, Gary L Miller, Richard Peng, and Charalampos E Tsourakakis. 2012. Efficient triangle counting in large graphs via degree-based vertex partitioning. *Internet Mathematics* 8, 1-2 (2012), 161–185.

[38] Longbin Lai, Lu Qin, Xuemin Lin, Ying Zhang, Lijun Chang, and Shiyu Yang. 2016. Scalable distributed subgraph enumeration. *Proceedings of the VLDB Endowment* 10, 3 (2016), 217–228.

[39] Jure Leskovec and Andrej Krevl. 2014. SNAP Datasets: Stanford large network dataset collection.

[40] Brenton Lessley, Talita Perciano, Manish Mathai, Hank Childs, and E Wes Bethel. 2017. Maximal clique enumeration with data-parallel primitives. In *2017 IEEE 7th Symposium on Large Data Analysis and Visualization (LDAV)*. IEEE, 16–25.

[41] Rong-Hua Li, Sen Gao, Lu Qin, Guoren Wang, Weihua Yang, and Jeffrey Xu Yu. 2020. Ordering heuristics for k-clique listing. *Proceedings of the VLDB Endowment* 13, 12 (2020), 2536–2548.

[42] Wenqing Lin, Xiaokui Xiao, Xing Xie, and Xiao-Li Li. 2016. Network motif discovery: A GPU approach. *IEEE transactions on knowledge and data engineering* 29, 3 (2016), 513–528.

[43] Amogh Lonkar and Scott Beamer. 2021. Accelerating Clique Counting in Sparse Real-World Graphs via Communication-Reducing Optimizations. *arXiv preprint arXiv:2112.10913* (2021).

[44] Zhenqi Lu, Johan Wahlström, and Arye Nehorai. 2018. Community detection in complex networks via clique conductance. *Scientific reports* 8, 1 (2018), 1–16.

[45] Vikram S Maitlody, Ketan Date, Zaid Qureshi, Carl Pearson, Rakesh Nagi, Jinjun Xiong, and Wen-mei Hwu. 2018. Collaborative (CPU+GPU) algorithms for triangle counting and truss decomposition. In *2018 IEEE High Performance extreme Computing Conference (HPEC)*. IEEE, 1–7.

[46] Samuel Manoharan. 2020. Patient Diet Recommendation System Using K Clique and Deep learning Classifiers. *Journal of Artificial Intelligence* 2, 02 (2020), 121–130.

[47] Duane Merrill. 2015. Cub. *NVIDIA Research* (2015).

[48] Rasmus Pagh and Charalampos E Tsourakakis. 2012. Colorful triangle counting and a mapreduce implementation. *Inform. Process. Lett.* 112, 7 (2012), 277–281.

[49] Santosh Pandey, Xiaoye Sherry Li, Aydin Buluc, Jiejun Xu, and Hang Liu. 2019. H-index: Hash-indexing for parallel triangle counting on GPUs. In *2019 IEEE High Performance Extreme Computing Conference (HPEC)*. IEEE, 1–7.

[50] Carl Pearson, Mohammad Almasri, Omer Anjum, Vikram S Maitlody, Zaid Qureshi, Rakesh Nagi, Jinjun Xiong, and Wen-mei Hwu. 2019. Update on triangle counting on GPU. In *2019 IEEE High Performance Extreme Computing Conference (HPEC)*. IEEE, 1–7.

[51] Marco Pellegrini, Miriam Baglioni, and Filippo Geraci. 2016. Protein complex prediction for large protein protein interaction networks with the Core&Peel method. *BMC bioinformatics* 17, 12 (2016), 37–58.

[52] Ali Pinar, C Seshadhri, and Vaidyanathan Vishal. 2017. Escape: Efficiently counting all 5-vertex subgraphs. In *Proceedings of the 26th international conference on world wide web*. 1431–1440.

[53] Ryan A. Rossi and Nesreen K. Ahmed. 2015. The Network Data Repository with Interactive Graph Analytics and Visualization. In *AAAI*. <http://networkrepository.com>

[54] Ryan A Rossi and Rong Zhou. 2018. Graphzip: a clique-based sparse graph compression method. *Journal of Big Data* 5, 1 (2018), 1–14.

[55] Ryan A Rossi and Rong Zhou. 2019. System and method for compressing graphs via cliques. US Patent 10,217,241.

[56] Ryan A Rossi, Rong Zhou, and Nesreen K Ahmed. 2018. Estimation of graphlet counts in massive networks. *IEEE transactions on neural networks and learning systems* 30, 1 (2018), 44–57.

[57] Matthew C Schmidt, Nagiza F Samatova, Kevin Thomas, and Byung-Hoon Park. 2009. A scalable, parallel algorithm for maximal clique enumeration. *J. Parallel and Distrib. Comput.* 69, 4 (2009), 417–428.

[58] Jessica Shi, Laxman Dhulipala, and Julian Shun. 2020. Parallel clique counting and peeling algorithms. *arXiv preprint arXiv:2002.10047* (2020).

[59] Zhiao Shi, Catherine K Derow, and Bing Zhang. 2010. Co-expression module analysis reveals biological processes, genomic gain, and regulatory mechanisms associated with breast cancer progression. *BMC systems biology* 4, 1 (2010), 1–14.

[60] Trevor Steil, Tahsin Reza, Keita Iwabuchi, Benjamin W Priest, Geoffrey Sanders, and Roger Pearce. 2021. TriPoll: computing surveys of triangles in massive-scale temporal graphs with metadata. In *Proceedings of the International Conference for High Performance Computing, Networking, Storage and Analysis*. 1–12.

[61] Etsuji Tomita, Akira Tanaka, and Haruhisa Takahashi. 2006. The worst-case time complexity for generating all maximal cliques and computational experiments. *Theoretical computer science* 363, 1 (2006), 28–42.

[62] Ha-Nguyen Tran, Jung-jae Kim, and Bingsheng He. 2015. Fast subgraph matching on large graphs using graphics processors. In *International Conference on Database Systems for Advanced Applications*. Springer, 299–315.

[63] Phonexay Vilakone, Doo-Soon Park, Khamphaphone Xinchang, and Fei Hao. 2018. An efficient movie recommendation algorithm based on improved k-clique. *Human-centric Computing and Information Sciences* 8, 1 (2018), 1–15.

[64] Leyuan Wang and John D Owens. 2019. Fast bfs-based triangle counting on GPUs. In *2019 IEEE High Performance Extreme Computing Conference (HPEC)*. IEEE, 1–6.

[65] Leyuan Wang and John D Owens. 2020. Fast Gunrock Subgraph Matching (GSM) on GPUs. *arXiv preprint arXiv:2003.01527* (2020).

[66] Leyuan Wang, Yangzihao Wang, and John D Owens. 2016. Fast parallel subgraph matching on the GPU. In *HPDC*.

[67] Leyuan Wang, Yangzihao Wang, Carl Yang, and John D Owens. 2016. A comparative study on exact triangle counting algorithms on the GPU. In *Proceedings of the ACM Workshop on High Performance Graph Processing*. 1–8.

[68] Pinghui Wang, Junzhou Zhao, Xiangliang Zhang, Zhenguo Li, Jiefeng Cheng, John CS Lui, Don Towsley, Jing Tao, and Xiaohong Guan. 2017. MOSS-5: A fast method of approximating counts of 5-node graphlets in large graphs. *IEEE Transactions on Knowledge and Data Engineering* 30, 1 (2017), 73–86.

[69] Yi-Wen Wei, Wei-Mei Chen, and Hsin-Hung Tsai. 2021. Accelerating the Bron-Kerbosch algorithm for maximal clique enumeration using GPUs. *IEEE Transactions on Parallel and Distributed Systems* 32, 9 (2021), 2352–2366.

[70] Lei Yang, Xudong Zhao, and Xianglong Tang. 2014. Predicting disease-related proteins based on clique backbone in protein-protein interaction network. *International journal of biological sciences* 10, 7 (2014), 677.

[71] Haiyuan Yu, Alberto Paccanaro, Valery Trifonov, and Mark Gerstein. 2006. Predicting interactions in protein networks by completing defective cliques. *Bioinformatics* 22, 7 (2006), 823–829.

[72] Ting Yu and Mengchi Liu. 2017. A linear time algorithm for maximal clique enumeration in large sparse graphs. *Inform. Process. Lett.* 125 (2017), 35–40.

[73] Ting Yu and Mengchi Liu. 2019. A memory efficient maximal clique enumeration method for sparse graphs with a parallel implementation. *Parallel Comput.* 87 (2019), 46–59. <https://doi.org/10.1016/j.parco.2019.07.001>.

05.005

1109/ICDE48307.2020.00112

[74] L. Zeng, L. Zou, M. T. Özsü, L. Hu, and F. Zhang. 2020. GSI: GPU-friendly Subgraph Isomorphism. In *2020 IEEE 36th International Conference on Data Engineering (ICDE)*. 1249–1260. <https://doi.org/10.1109/ICDE48307.2020.00112>.